ARTICLE

Effects of the Nanostructuring of Gold Films upon Their Thermal Stability

Michael Bowker,[†,*] Albert F. Carley,[†] Philip R. Davies,[†] David J. Morgan,[†] Jonathan Crouch,[†] Georgi Lalev,[‡] Stefan Dimov,[‡] and Duc-Truong Pham[‡]

[†]Wolfson Nanoscience Laboratory, School of Chemistry, Cardiff University, Cardiff CF10 3AT, U.K. and [‡]Manufacturing Engineering Centre, Cardiff University, Queen's Buildings, The Parade, Newport Road, Cardiff CF24 3AA, U.K.

ABSTRACT We report results relating to the thermal stability of nanoparticles and show a remarkable effect of nanostructuring of the metal. Au films are nanostructured by focused ion beam sputtering (FIB) to produce isolated areas of metal, which are imaged by atomic force microscopy (AFM). Images of the surface show that, if the islands are made small enough, the metal in the islands is lost by evaporation, whereas the nonfabricated areas outside are relatively stable and the nanoparticles remain present there.

KEYWORDS: FIB · gold nanoparticles · nanostructured gold films · thermal stability of nanoparticles · vaporization · nanoparticle imaging · AFM

Nanoparticulate materials are already very important for modern technology, and they will only increase in their application in the coming years. As a result of the nanoscience revolution, there has been increasing interest in the fabrication, characterization, and properties of nanoparticles. However, much of the work is carried out on nanomaterials prepared at, or close to, ambient temperature, whereas there are many areas of technology where thermal stability is a crucial aspect of the application, for instance, in heterogeneous catalysis[1,2] and fuel cells.[3] In some cases, such materials have to operate above 1000 K, and the active phase often consists of metal particles on a ceramic support, materials of the type presented in this paper.

Surfaces are regions of high energy, and this property has consequences for the stability of nanoparticles and for a variety of areas of technology. Because of this high energy, which exists due to the undercoordination of surface atoms compared with those in the bulk, surfaces tend to minimize surface energy in a variety of ways. This includes changes in nanoparticle morphology (minimization of surface area by tending to a spherical shape and by minimization of high-energy crystal planes) and particle aggregation in order to reduce surface area (sintering). In technological areas, such as heterogeneous catalysis, where it is essential to maintain the surface area in order to retain high catalytic activity, such sintering is reduced by anchoring the metal nanoparticles involved onto refractory supports such as alumina, and this is achieved during the synthesis of the material. Preparation of such materials generally involves a "calcination" step (heating to elevated temperature) in order to decompose the precursor material and form metallic nanoparticles.

In the present work, we report the effects of nanostructuring upon the behavior of nanoparticles, especially on their thermal stability, in a rather direct way, by imaging Au films deposited on an alumina single crystal and their structural evolution with annealing temperature.

RESULTS AND DISCUSSION

Gold arrays can be made in a whole variety of ways, both using "bottom-up" methods (see, for instance, refs 4 and 5) and "top-down" methods.[6] We have made films of gold, produced by metal vapor deposition (MVD) onto an alumina (0001) single crystal, and have nanostructured them using focused ion bombardment (FIB), a top-down method. XPS analysis of such a film before annealing (Figure 1) shows that the substrate alumina signal has essentially disappeared after film deposition, indicative of the formation of a film of gold covering the whole surface. By AFM and scanning electron microscopy (SEM) analysis, the thickness of the film is ~15 nm.

FIB is most often used for machining structures to small size for use by other techniques such as transmission electron microscopy (TEM) or SEM.[7] It is much less

*Address correspondence to bowkerm@cf.ac.uk.

Received for review November 12, 2009 and accepted February 28, 2010.

Published online March 5, 2010. 10.1021/nn901614e

often used for nanostructured array formation,[8] EBL (electron beam lithography) being used more frequently,[6] though usually not directly (*i.e.*, using masks of various kinds). However, here the films described above were engineered into several types of structures by machining lines through the film using the FIB method.[9−11] Examples of the structures formed are shown in Figure 2, imaged by AFM (Veeco Multimode with Nanoscope IIIa controller). The fabricated areas only occupy a very small part of the 10 × 10 mm crystal, each being around 30 μm^2. The deposited film consists of a somewhat grainy layer of Au on the alumina (Supporting Information Figure S1), which arises from the Volmer−Weber-type growth of metals on such oxides.[12−15] In this growth mode, the higher surface energy of the metal compared to the oxide results in nucleation and island growth, with the monolayer forming as islands coalesce. This graininess could indicate some porosity in the film, but such porosity is very limited because XPS (X-ray photoelectron spectroscopy) analysis of the film shows no evidence of any signal from the alumina crystal beneath it, as expected for a continuous film of this thickness (Figure 1). There are two types of machined structures shown in Figure 2, both of which consist of ~40 nm lines cut into the Au film by FIB, with an average spacing between them of 350 nm. One structure simply consists of these lines fabricated over an area of 5 μm × 6 μm, whereas the other consists of orthogonal lines, leaving isolated cells of Au of ~250 nm × 250 nm, though, as can be seen in Figure 2, there is some variation in the size of these cells (~10%). Line scans show that the structured areas are rougher than the film, the mean roughness of the former being ~15 nm, while it is less than 1 nm for the unstructured areas. Some damage also occurs to the film itself, due to the FIB; some swelling of the remaining Au film occurs (see, for instance, the edges of the gold lines in Figure 2), and this is a well-documented effect of such treatment.[16] Furthermore, it is clear that the machined areas of the Au film are somewhat more porous than the unstructured film (see the cells in Figure 2), probably due to ion beam damage. Nonetheless, it is evident that there are clear lines where the sputtering has taken place, and imaging after heating at very high temperature, when all the gold has been removed, shows that this sputtering takes place right through the gold film and into the alumina beneath (see Figure 4).

The main aim here was to investigate the effect of thermal treatment upon the three types of film (that is, the two structured areas plus the unstructured film). Upon heating to 1173 K for 3 h (Figure 3), it is clear that the film has changed significantly and that it has separated into nanoparticles. It is apparent from these images that (i) the particles in the nanostructured areas are generally smaller than those in the rest of the film and (ii) the particles in the structured areas remain located within the prefabricated structures. The majority of the particles for the structured films are less than 500 nm in perimeter length (for the cell structures, 80% are less than this value, with a mean particle size of 95 nm; particle size distribution plots are given in the Supporting Information Figure S2), whereas for the unstructured film, most are bigger than this (78%, mean particle size ~250 nm). Thus, nanostructuring of the film by FIB has had a major effect on the thermal evolution of the structure of the treated areas.

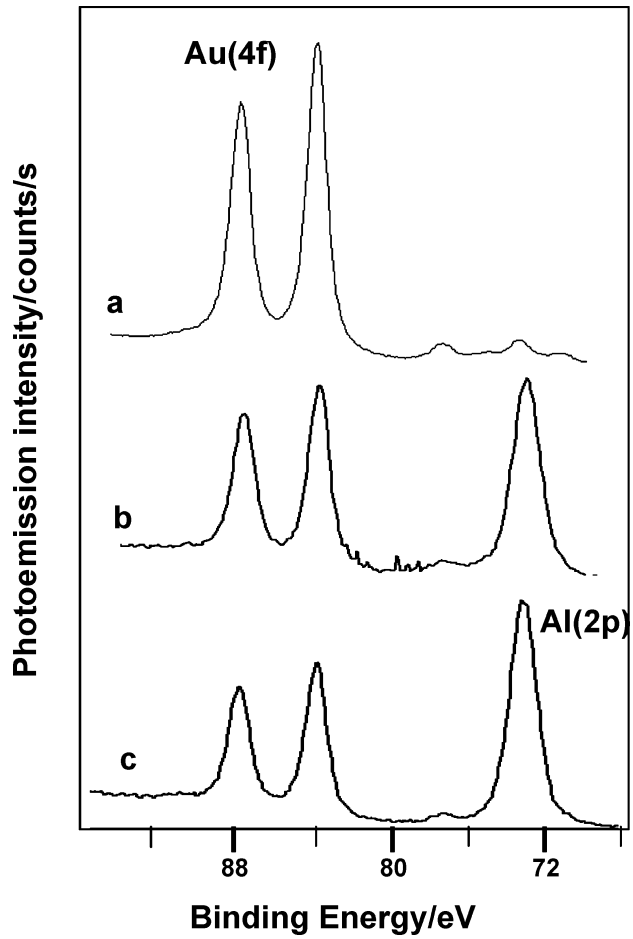

Figure 1. XP spectra for (a) the as-prepared sample and (b) after heating to 900 °C and (c) 1100 °C. Note that the peaks in the 70−80 eV region in (a) are due to satellite lines from the main Au(4f) peaks. The signal from the alumna substrate is only seen after heating because the sputtered areas are only a tiny fraction of the total area analyzed by XPS before heating, whereas the alumina is exposed over the whole surface after heating due to dewetting of the surface by gold.

These observations are associated with the creation of artificial boundaries within the gold film, from which material retreats during annealing due to dewetting of the underlying alumina. Note that from other studies[15] we have identified that these transformations begin to take place at around the Tamman temperature (~670 K for Au), which is often associated with the onset of mobility within solids. There is also some evidence that particles within the cells are somewhat smaller than those even within the fabricated parallel line structures. There

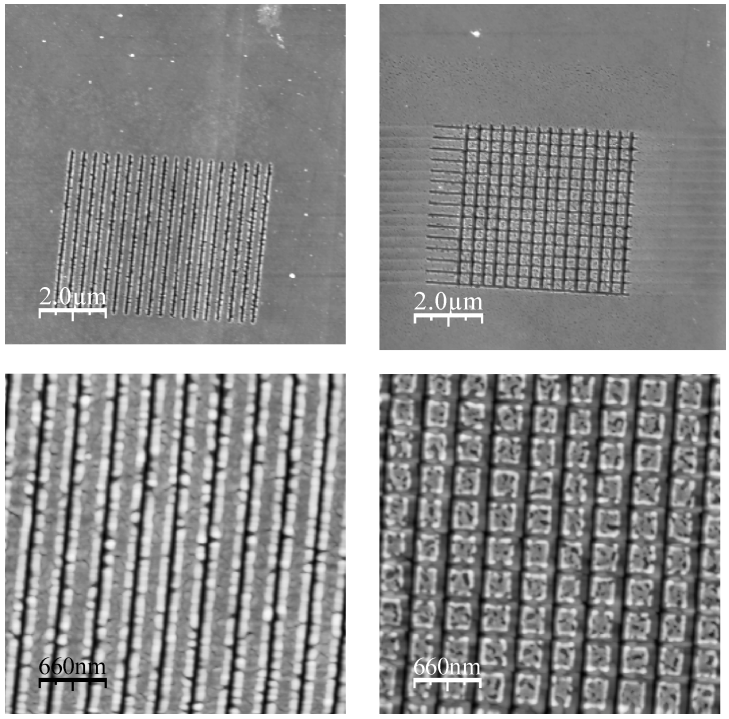

Figure 2. AFM images of two nanostructured areas on the gold film. On the left side, lines are sputtered into the surface, whereas on the right, we have orthogonal sputtered lines producing isolated islands of Au.

is little evidence of sintering after dewetting because the particle size distribution changes very little upon heating between 973 and 1173 K. This is due to the very large interparticle separation that minimizes the coalescence and Ostwald ripening type sintering that is observed for much smaller particles that are packed together more closely.[14,15]

However, perhaps the most important finding here relates to Au evaporation from the surface while heating to 1373 K (Figure 4); there is very little loss of gold from the surface at 1173 K, but there is at 1373 K. Here, it is very clear that Au is completely lost from the cells but not from the unstructured area, where the average particle size is still around 200 nm, though the particle size distribution has broadened considerably and the number density has decreased somewhat. The area machined with lines also has some particles present, but much fewer than for the unstructured film. Thus, nanostructuring enhances evaporation rates for nanoparticles. Imaging of such an effect has not been reported before, but it is a reflection of the nature of the nanoparticles formed—on the nanostructured areas, they are significantly smaller than for the unstructured areas. This is confirmed by observations of cells of larger size (Supporting Information Figure S3), where (i) the Au particles in these 1 μm cells are larger than for the smaller cells before heating to 1373 K and (ii) particles still remain after heating to 1373 K.

To understand this behavior, we might consider that this may be a reflection of the increased surface energy for small particles, which in turn is a reflection of lower average surface coordination and hence a lower energy barrier to vaporization. However, from considerations of average surface coordination (see Supporting Information), it is evident for particles of the size shown in Figures 3 and 4 that the surface energy is not significantly different between particles of ~100 nm (in the cells) and ~250 nm diameter (in the unstructured film). Indeed, the surface is essentially macroscopic in its behavior, with average surface coordination very close to 9 for both types of nanoparticles. Significant lowering of the average surface coordination only occurs for particles smaller than 5 nm or so in diameter. So it is not *mainly* a surface energy difference that leads to the marked effects of Figure 4, though we will return to this point below.

The main reason that nanostructuring has such a marked effect is that it produces smaller particles after heating which have a higher surface/bulk ratio. This means that the rate of loss of material from the surface of the particle is high compared with its bulk volume; that is, it runs out of material more rapidly, and hence, such particles disappear before the larger particles do. We can approximate these rates in the following way and by use of bulk data for the evaporation process

$$-d[\mathrm{Au}]/dt = k_e[\mathrm{Au_s}] = k_e' 2\pi r^2 \qquad (1)$$

where the left-hand side represents the rate of loss of gold from a particle; k_e is the evaporation rate constant from the Au particle, and this is multiplied by the amount of surface Au available for evaporation. This is, in turn, represented on the right-hand side of eq 1 in terms of surface area and $k_e' = k_e N_s$, where N_s, the sur-

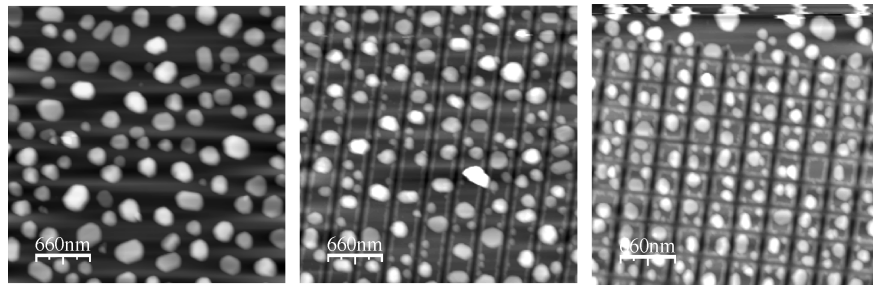

Figure 3. Effects of annealing to 1173 K on the structure of the unprocessed area (left), the lined area (middle), and the area with cellular structure (right).

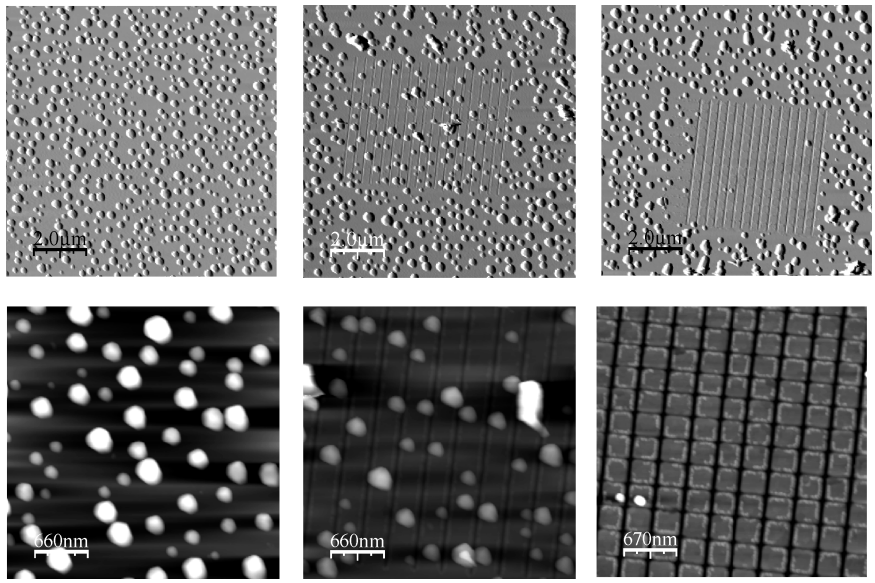

Figure 4. Effect of heating to 1373 K for 3 h on the structure of the unprocessed area (left), the lined areas (middle), and the cells (right). Almost all of the gold has been lost from the cellular area.

face concentration of Au atoms, can be expressed in terms of atoms m^{-2} or monolayers. What we would like to know, in terms of the experiments shown in Figures 3 and 4, is the rate of decrease of radius with time in order to compare the rates from small and large nanoparticles. Substituting for the particle volume (proportional to the total amount of gold), we obtain

$$-dV/dt = k'_e\rho 2\pi(3V/2\pi)^{2/3} = kV^{2/3} \quad (2)$$

where $k = k_e'\rho 3^{2/3}(2\pi)^{1/3}$, where ρ is the density of gold. Upon integration, the time evolution of volume is given as

$$V_t^{1/3} = V_0^{1/3} - kt/3 \quad (3)$$

which can be expressed again in terms of particle radius

$$r_t = r_0 - k'_e\rho t \quad (4)$$

that is, there is a zero-order dependence of radius upon time. Thus, if we consider two particles, one twice the size of the other, then the smaller one will have disappeared when the larger one has only decreased in size by a factor of 2. We can estimate the absolute rate of loss of radius if we can evaluate the rate constant above, which can be expanded in the usual Arrhenius form.

$$k' = A' \exp(-E/RT) \quad (5)$$

The E value is the activation energy for vaporization, which is reported to be 324 kJ mol^{-1},[17] and as described above, these large nanoparticles are essentially bulk-like in their behavior and so it is reasonable to assume that the bulk heat of vaporization applies. The estimate of the vaporization indicates that rates are insignificant in terms of the experiments above at less than ~1300 K. However, at 1373 K, the evaporation rate is ~0.05 monolayers s^{-1} (or approximately 0.01 nm s^{-1}), so a particle of 100 nm diameter will be lost in $\sim 10^4$ s (which is the period of heating in this case), whereas clearly it will take longer for the bigger particles.

In conclusion, we have shown that nanostructuring of gold films has a marked effect on nanoparticle formation and the effect of thermal treatment on such particles. The nanostructuring creates artificial, extra boundaries, which lead to the formation of smaller nanoparticles as the film dewets with annealing to high temperature. Perhaps more importantly, this strongly affects evaporation rates, with the smaller nanoparticles evaporating away from the surface at a much faster rate than for larger particles. This may have important consequences for the processing of films and nanoparticle arrays in a variety of technological areas which may involve high-temperature treatments.

METHODS

The sample used as the basis for deposition was an alumina (0001) single crystal of 5N purity. The preparation of the nanostructured sample first involved the deposition of a thin layer of Au onto the single crystal of alumina. This was achieved by resistive evaporation in which a sample of Au wire was placed in a tungsten evaporation boat and mounted in a thermal resistive evaporator. The film thickness was monitored during the deposition process using a precalibrated crystal monitor, and the thickness of the film used here was ~15 nm.

The next stage in the crystal preparation involves focused ion beam (FIB, Carl-Zeiss XB 1540) machining in order to fabricate the various patterns into the crystal, using gallium ions,

which sputter the Au film and alumina beneath the film. The FIB system is controlled externally by Eliphy Quantum lithography software and hardware package, which facilitate the design of the pattern to be etched and control the dwell time of the ion beam at each individual pixel, step size between the pixels, number of loops, *etc*. The sample was inspected *in situ* during the milling process using a high-resolution field emission scanning electron (FE SEM) microscope integrated into the FIB system. In this particular study, the trenches were milled into alumina with a pitch of 400 nm and width of 75 nm. Note that the data presented here are from ONE sample, with all the different fabricated structures being on the same crystal substrate. This ensures that when comparing structure effects they are for areas treated at EXACTLY the same temperature and conditions. They were imaged by AFM (Veeco Multimode with Nanoscope IIIa controller), using a contact mode tip, as the alumina surfaces were hard enough to withstand the force exerted by this mode of operation. Some more details are given in the Supporting Information.

Acknowledgment. This work was partly funded by EPSRC and Cardiff University

Supporting Information Available: AFM images, particle size distributions, and other information. This material is available free of charge *via* the Internet at http://pubs.acs.org.

REFERENCES AND NOTES

1. Parker, S.; Campbell, C. T. Kinetic Model for Sintering of Supported Metal Particles. *Phys. Rev. B* **2007**, *75*, 035430-1–035430-15, and references therein.
2. Bell, A. T. The Impact of Nanoscience on Heterogeneous Catalysis. *Science* **2003**, *299*, 1688–1689.
3. Ding, J.; Liu, J. Fabrication and Electrochemical Performance of Anode-Supported Solid Oxide Fuel Cells by a Single-Step Co-Sintering Process. *J. Am. Ceram. Soc.* **2008**, *91*, 3303–3307.
4. Lundgren, A.; Bjorefors, F.; Olofsson, L.; Elwing, H. Self-Arrangement Among Charge-Stabilized Gold Nanoparticles on a Dithiothreitol Reactivated Octanedithiol Monolayer. *Nano Lett.* **2008**, *8*, 3989–3992.
5. Zheng, J.; Constantinou, P. E.; Micheel, C.; Alivisatos, A. P.; Kiehl, R. A.; Seeman, N. C. Two-Dimensional Nanoparticle Arrays Show the Organizational Power of Robust DNA Motifs. *Nano Lett.* **2006**, *6*, 1502–1504.
6. Smythe, E.; Dickey, M.; Whitesides, G. M.; Capasso, F. A Technique to Transfer Metallic Nanoscale Patterns to Small and Non-Planar Surfaces. *ACS Nano* **2009**, *3*, 59–65.
7. Rowland, C.; King, W.; Cross, G.; Pethica, J. B. Measuring Glassy and Viscoelastic Polymer Flow in Molecular-Scale Gaps Using a Flat Punch Mechanical Probe. *ACS Nano* **2008**, *2*, 419–428.
8. Tong, H. D.; Jansen, H. V.; Gadgil, V. J.; Bostan, C. G.; Berenschot, E.; van Rijn, C. J.; Elwenspoek, M. Silicon Nitride Nanosieve Membrane. *Nano Lett.* **2004**, *4*, 283–287.
9. Tseng, A. A.; Insua, I.; Park, J.-S.; Chen, C. D. Milling Yield Estimation in Focussed Ion Beam Milling of Two Layer Substrates. *J. Micromech. Microeng.* **2004**, *15*, 20–28.
10. Li, W.; Dimov, S.; Lalev, G. Focused Ion Beam Direct Structuring of Fused Silica for Fabrication of Nanoimprinting Templates. *Microelectron. Eng.* **2007**, *84*, 829–832.
11. Li, W.; Lalev, G.; Dimov, S.; Zhao, H.; Pham, D. T. A Study of Fused Silica Micro/Nano Patterning by Focussed Ion Beam. *Appl. Surf. Sci.* **2007**, *253*, 3608–3614.
12. Freund, H.-J.; Pacchioni, G. Oxide Ulrathin Films on Metals. *Chem. Soc. Rev.* **2008**, *37*, 2224–2242.
13. Chatain, D.; Coudurier, L.; Eustathopoulos, N. Wetting and Interfacial Bonding in Ionocovalent Oxide-Liquid Metal Systems. *Rev. Phys. Appl.* **1988**, *23*, 1055–1064.
14. Bowker, M. Adventures in Catalytic Nanospace: Resolving Catalytic Phenomena with STM. *Phys. Chem. Chem. Phys.* **2007**, *9*, 3514–3521.
15. Stone, P.; Poulston, S.; Bennett, R. A.; Bowker, M. STM Investigation of Sintering in a Model Supported Catalyst: Nanoscale Pd on TiO_2. *Chem. Commun.* **1998**, 1369–1370.
16. Menzel, R.; Bachmann, T.; Machalett, F.; Wesch, W.; Lang, U.; Wendt, M.; Musil, C.; Muhle, R. Surface Smoothing and Patterning of SiC by Focussed Ion Beams. *Appl. Surf. Sci.* **1998**, *136*, 1–7.
17. *Handbook of Chemistry and Physics*, 82nd ed.; CRC Press: Washington, DC, 2001; pp 6−106.